NUMERICAL ANALYSIS OF FLUID FLOW THROUGH FIBROUS POROUS MATERIALS

U. Aaltosalmi[1], M. Kataja[1], A. Koponen[2], J. Timonen[1], A. Goel[3], G. Lee[3], and S. Ramaswamy[3]

[1]Department of Physics, PB 35 (YFL) FIN-40014 University of Jyväskylä, Finland

[2]VTT Processes, PB 1603 FIN-40101, Jyväskylä, Finland

[3]Department of Wood and Paper Science, University of Minnesota, St. Paul, MN, USA

ABSTRACT

X-ray microtomography, numerical structure generation, 3D image analysis and lattice-Boltzmann flow simulations are used in analyzing flow in fibrous porous materials. We determine the flow permeability and other flow related parameters for three-dimensional structures given by x-ray tomographic images of paper samples, and also for structures generated by the PAKKA fibre-deposition model. Comparison with experimental permeabilities is included. Properly combined, the novel experimental and numerical methods utilized here can provide very effective tools for the study of various structural and transport properties of paper, board and paper-making fabrics.

INTRODUCTION

Paper, paperboard and paper-making fabrics are complex three-dimensional bi-continua of interconnected pores and fibrous solid material. Transport properties such as liquid permeability, vapor diffusivity and thermal conductivity in such porous media are inherently related to the resistance offered by the three-dimensional structure. Moisture conduction in paper and fabrics is central to many process operations such as drainage of a wet paper web, its subsequent dewatering under vacuum and pressure, and finally to its drying behavior. In general, the transport and structural properties of fibrous porous materials relevant to paper making can only be found experimentally. Lately, also direct numerical simulations have been used in studying the mesoscopic-scale dynamics underlying the observed macroscopic transport properties [1-5]. The basic problem in such simulations is an adequate description of the pore structure. Since practical experimental methods for finding the actual structure have not been available until quite recently, numerical algorithms have been developed for generating model structures for various fibrous materials. These models have been successfully applied especially for fabrics and artificially made fibrous filters [6,7]. Numerical model structures, although they capture many essential features of real paper, should not however be considered as *exact* models of paper as for their transport properties. No attempt was thus made here to model the paper samples used with the numerically generated PAKKA structures, whose role is to represent rather generic paper-like fibrous structures.

X-ray microtomography is a novel technique used in three-dimensional imaging of materials. This method consists of obtaining a large set of images while passing radiation through the sample at different angles. The projected images can be combined so as to reconstruct the geometry of the interior structure. Since cellulose and the surrounding medium have approximately equal absorptivities for x-rays, the "phase-contrast method", instead of the traditional "absorptive-contrast method" used in medical applications, is preferred in imaging *e.g.* paper and board. Samuelsen et.al. [8,9], Guruyev et.al. [10] and Goel et al. [11] have demonstrated the use of phase contrast imaging in paper.

In this work we demonstrate the usefulness of several novel methods, namely x-ray microtomography, numerical structure generation, 3D image analysis and lattice-Boltzmann numerical simulations, for analysing transport related properties of paper-like materials. We show results from numerical flow simulation through fibrous structures created by the PAKKA random-deposition model [6] and through actual paper samples using their 3D x-ray tomographic images. In addition, flow permeability, porosity, specific pore surface and tortuosity of the paper samples are estimated using tailored image analysis algorithms. Both transverse and in-plane flows are considered in each case.

THEORY

At low Reynolds numbers, fluid flow through porous medium is well described by Darcy's law [12],

$$\vec{q} = -\frac{k}{\mu}\vec{\nabla} p \,, \tag{1}$$

where $\vec{q}$ is the flow velocity, μ the dynamic viscosity of the fluid, and p the fluid pressure. The permeability coefficient k measures the conductivity to fluid flow of the porous material, and is *a priori* unknown. Apparently, the most widely used expression that relates permeability to the relevant structural characteristics of the porous material, is the Kozeny-Carman equation [11],

$$k = \frac{1}{c\tau^2 S_0^2}\frac{\phi^3}{(1-\phi)^2}\,. \tag{2}$$

Here ϕ is the porosity, S_0 the specific surface area (i.e., pore-surface area in a unit volume of the solid material), τ the tortuosity (i.e., the ratio of the average length of the flow paths to the thickness of the sample), and c the dimensionless Kozeny's constant. A number of similar formulae, derived especially for fibrous porous materials, can be found in the literature (see e.g. an extensive review by Jackson and James [13]). An example of such a formula, derived by Happel for an array of parallel cylindrical rods perpendicular to flow, is given by [14]

$$k = \frac{a^2}{8\varphi}\left(-\ln\varphi + \frac{\varphi^2 - 1}{\varphi^2 + 1}\right). \tag{3}$$

Here a is the average radius of the fibres and $\varphi = 1-\phi$ the solid volume fraction. In spite of their apparent dissimilarity, the qualitative behavior of the two permeability correlations as a function of ϕ, as given by Eqs. (2) and (3), is very similar for porosities $\phi \le 0.5$ (assuming constant τ in Eq. (2)). In particular, they share the common asymptotic behavior in that $k \propto \phi^3$ as $\phi \to 0$. Yet another formula based on numerical simulations is given by Koponen et. al. [4],

$$k = 5.55a^2\left[e^{10.1(1-\phi)} - 1\right]^{-1}. \quad (4)$$

The result Eq. (4) was derived to explain the transverse permeability of PAKKA-model samples, while the Happel formula Eq. (3) is just a theoretical construction for a regular array of rods. Neither of these two analytical results is thus specifically meant to describe the permeability of real paper, and the same is of course true for the Kozeny-Carman result Eq. (2). We use them here as they are relatively simple expressions and able to adequately describe the permeability of at least some materials.

METHODS

Paper samples. Hand sheets of a basis weight of 300 g/m^2 were prepared from bleached softwood kraft pulp. Pulp was beaten to six different refining levels, *viz*. 670, 570, 460, 330, 280, and 220 CSF in a laboratory beater. X-ray micro-computed tomographic imaging and 3D reconstruction of the images of samples of varying structure were done with a Sky-Scan-1072 system developed and manufactured by SkyScan, Belgium. The resolution and the size of the images were about 2 μm and 1 mm^2, respectively. The final samples used in the lattice-Boltzmann simulations were obtained from the original samples by removing their uneven surface layers in the direction perpendicular to the transverse (z) axis. The thicknesses of the final samples thus obtained varied between 120 μm and 200 μm. Image analysis tools were developed to characterize the 3D structural parameters of the samples, namely porosity, fibre-void interfacial area (specific surface area) and pore-size (hydraulic-radius) distribution in two orthogonal directions [11,15]. Reasonable comparisons with conventional mercury intrusion porosimetry data from the same samples were obtained [15].

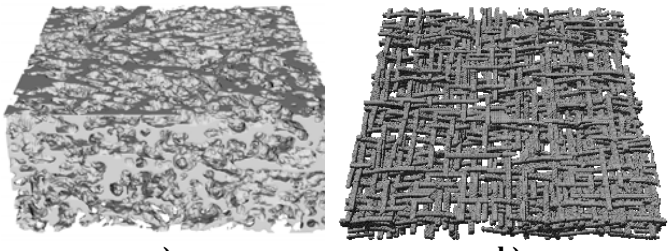

a) **b)**

Figure 1: a) A tomographic image of paper sample CSF 670. Shown is 1/4 of the sample used in the analysis. b) A fibre structure created by the PAKKA model.

PAKKA model structures. Within the numerical PAKKA model [6], fibre webs are grown by randomly depositing flexible fibres of rectangular cross section on a flat substrate. These webs are periodic in the in-plane (*x* and *y*) directions. The surfaces perpendicular to the z axis were removed similarly to the paper samples. The porosity of the samples is controlled by varying the flexibility of the deposited fibres. In this version of the model, fibres are randomly oriented in two perpendicular directions. The fibre width to length ratio is 1:20, and the size of the samples is four fibre lengths in the *x* and *y* directions and ten fibre widths in the *z* direction. The structures have been discretized for the lattice-Boltzmann simulations with fibre widths of 5, 10 or 20 lattice units.

Examples of structures generated by tomographic imaging of actual paper samples and by the PAKKA model are shown in Fig. 1.

Lattice-Boltzmann hydrodynamics. The lattice-Boltzmann (LB) method [1,2] is a novel mesoscopic approach to computational fluid dynamics. It has been successfully applied to many complicated flow problems such as flows of particulate suspensions and fluid flows in porous media [3-5]. In this method fluid is modelled by particle distributions that move on a regular lattice. At each time step particles propagate to their adjacent lattice points, and re-distribute their momenta in the subsequent collisions. Hydrodynamic quantities such as density and velocity are obtained from the velocity moments of the distribution function. Here, we use the three-dimensional 19-link (D3Q19) LBGK (lattice-Bhatnagar-Gross-Krook) model, where the collision operator is based on a single-time relaxation to the local equilibrium distribution. The Stokesian fluid flow in the pore space is generated by a uniform external body-force density that equals the mean pressure gradient. At solid-fluid interfaces we have realized the no-slip boundary condition by the bounce-back rule, whereby the momenta of the particles that meet a solid wall are simply reversed.

Fluid-flow simulations. The LB simulations were done for the x-ray tomographic images of the six paper samples specified above and for porous samples created numerically with the PAKKA model. The fluid-flow simulations were carried out both in the in-plane and transverse directions to determine the anisotropy of permeability, which is an important quantity in many processes such as wet pressing. The effect on permeability of the fines content in real paper was estimated by using generic PAKKA model structures in which different amounts of randomly deposited small cubic particles were included on fibre surfaces. In addition to permeability, we determined the hydrodynamic (flux weighted) tortuosities [16] of the paper and PAKKA-model samples.

The boundary conditions imposed in the PAKKA-model simulations were selected so as to utilize the structural symmetry inherent in the model and to minimize the effects of the finite size of the samples. For the paper samples instead, the boundary conditions were selected to correspond to the experimental conditions, where appropriate. In the transverse-flow simulations, free fluid layers of at least 10% of the thickness of the sample were added above and below the sample, and periodic boundary conditions were imposed in the z direction. Periodic boundary conditions were imposed also in the x and y directions when simulating flow through the PAKKA model structures that are periodic in these lateral directions. In the case of the paper samples, the no-slip condition was used at the lateral boundaries. Notice, however, that the lateral dimensions of the samples were so large in comparison with their thickness that the choice of lateral boundary conditions had no significant effect on the transverse-flow results (see below).

For the in-plane flow simulations, free fluid layers were added at the boundaries perpendicular to the mean flow analogously with the transverse-flow case. In order to conform to the experimental set-up of the in-plane permeability measurements, the no-slip condition was used for the paper samples at all boundaries parallel to the mean flow. For the PAKKA model simulations, the frictionless slip condition was used at the boundaries perpendicular to the z direction, corresponding to reflection symmetry across these boundaries (to minimize the finite-size effects). With these boundary conditions no significant 'leakage' of fluid was observed along the boundaries.

In the current application, the numerical accuracy of the lattice-Boltzmann results is dominated by lattice resolution [2,3]. The effect on the simulated permeability of finite grid size was studied by varying the refinement of the computational lattice. The numerical error of the values obtained for permeability, due to this effect, was estimated to be less than 20 %. The effect of using different boundary conditions (slip, no-slip, periodic) was also studied. Here, the effect on the values obtained for the in-plane permeability was found to be less than 10%, and much less than that for the transverse permeability. We conclude that the primary source of uncertainty in the results reported below is the limited size of the paper samples (~ 1 mm^2) and the normal variation of paper material. In order to properly account for this 'formation effect', a large number of samples should be analyzed. Such a statistical approach was not possible at this stage as it would have demanded a large number of tomographic images.

Image analysis. In addition to direct LB flow simulations, we also estimated the permeability of the paper samples by using methods based on image analysis. Following the definition of tortuosity as the ratio of the actual pore length to the thickness of the porous material, the distribution of chord lengths passing through the porous structure were first determined using a numerical procedure described in Ref. [15]. The permeability of the samples was then calculated from Eq. (2) separately for the transverse and in-plane flows using porosity, specific surface area and tortuosity values obtained from the 3D-image analysis. The value $c = 2$ was used for the Kozeny constant. The errors in the image-analysis permeability estimates are approximately 20 %.

Experimental methods. For comparison, we also carried out experiments with the same paper grades as used in tomographic imaging. In this investigation, the in-plane water-flow characteristics of the paper samples were determined using a Liquid/Air Displacement Analyzer, originally developed by TRI/Princeton. The details of the experimental technique as applied to transverse and in-plane flow in polymeric fabrics are reported elsewhere [17]. The testing fixtures and test procedures were suitably modified to measure in-plane liquid-flow characteristics of paperboards.

The samples measured were conditioned under TAPPI standard method T-402. Both paper surfaces were covered with an impermeable plastic tape to prevent liquid from penetrating through the surface. The samples were cut to the final size of 8.3 x 4.8 cm. Three edges were sealed with glue and a hole was punched to apply pressure differential. The specimen was then mounted on a fixture and placed under water. Five different vacuum levels were applied through the hole. The volumetric rate of penetration of water, at a given applied pressure difference, was measured as a function of time by measuring weight loss of the whole system. From the volumetric rate of penetration, relative permeability and capillary pressure were calculated.

Due to the heterogeneous nature of paperboard, liquid front propagation during the test appeared uneven. This was expected and has been reported earlier [18]. In general, these results show that in-plane water flow in paper follows a general form of Darcy's law over a wide range of driving pressures. The correlation coefficients for the least-squares linear regression analysis of these data to Darcy's law ranged from 0.95 to 0.99. This range, for the variety of experimental conditions studied, supports the heterogeneous nature of paperboard. Also, under the range of driving pressures studied, the in-plane penetration of water in paperboard can be explained as a typical Newtonian creeping flow. These results indicate that the Liquid/Air Displacement Analysis test method based on Darcy's law can be used for characterizing in-plane liquid flow in paperboards. The estimated total error in the in-plane permeability measurements is approximately 20 %

RESULTS

X-ray tomographic images of paper samples. Table 1 summarizes some geometrical properties and results obtained from x-ray tomographic images of the six paper samples. The specific surface and porosity have been obtained from the image analysis, whereas the transverse and in-plane tortuosities have been determined both by image analysis (chord-length distribution algorithm [15]) and by LB flow simulations. Interestingly, paper sheets formed as strictly layered structures in the laboratory sheet mold show little change in tortuosity with changing porosity, as the fibres were refined and the density of the sheets was thereby increased. However, the transverse tortuosity seems to undergo a significant change with refining and densification indicating a more complex, less permeable structure. Notice that the chord-length method tends to give higher values for tortuosity, since the hydrodynamic tortuosity given by the LB method gives more weight to paths of least resistance, whereas the chord-length method does not prefer any particular fluid path or chord length.

Table 1: Structural properties of the six paper samples with varying refining level as given by image analysis; porosity ϕ, specific surface area S_0, transverse and in-plane tortuosities τ_{tr} and τ_{ip}, respectively. Also given are the hydrodynamic tortuosities given by LB simulations.

	Image analysis				LB	
CSF	ϕ	$S_0 / 10^6$ m^{-1}	τ_{tr}	τ_{ip}	τ_{tr}	τ_{ip}
670	0.43	0.168	2.04	1.33	1.57	1.37
570	0.36	0.148	3.19	1,50	1.96	1.30
460	0.31	0.144	3.32	1.46	2.16	1.44
330	0.29	0.135	3.58	1.58	2.99	1.20
280	0.26	0.129	3.92	2.01	2.60	1.65
220	0.25	0.121	5.34	2.20	2.29	1.68

In Fig. 2 we show the transverse and in-plane permeabilities of the paper samples as determined by LB simulations and by image analysis. Also shown are a few experimental results for the same paper grades [19]. Interestingly, with the selected value of Kozeny's constant, c = 2, the results obtained from image analysis are quite close to those of LB simulations. Both results also agree very well with the experimental value for the transverse air permeability of the CSF 670 sample. Unfortunately, at the time of writing, no other transverse permeability and air-flow results were available for these samples.

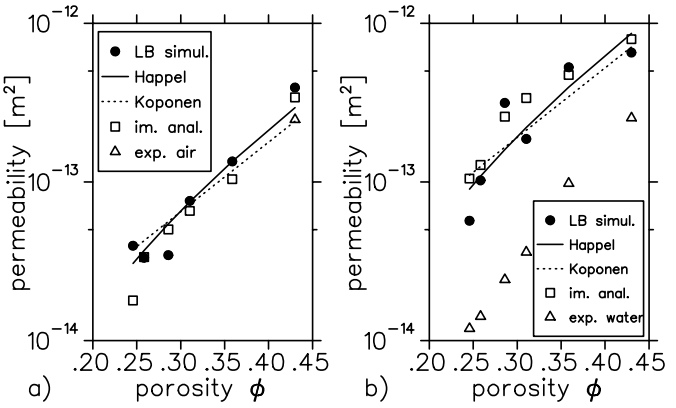

Figure 2: a) Transverse permeabilities of paper samples given by LB simulations, image analysis and one experimental point for air. b) In-plane permeabilities of paper samples given by LB simulations, image analysis and experimental values for water.

Comparing the computed and experimental values for the in-plane permeability shown in Fig. 2 b), a clear discrepancy can be seen. A plausible reason for this is that these experimental results were obtained using water, whereas dry samples were used in tomographic imaging. Due to swelling, the structure of the samples used in the experiments may not have been equivalent to those in tomographic imaging. Another reason that may have caused the computed permeability values to be above the experimental ones is the limited resolution of the tomographic images, which is still insufficient to resolve the complex microstructure of fibre surfaces. Thus, the specific surface obtained from the image analysis, and the flow resistance given by the LB simulations, may be underestimated.

Also shown in Figs 2 a) and b) are curves obtained by fitting Eqs. (3) and (4) to the LB results, using fibre radius a as a fitting parameter. For the transverse permeability, Fig. 2 a), the fitted values are a =5.05 μm and a =2.25 μm for Eqs. (3) and (4), respectively. For the in-plane permeability, Fig. 2 b), the corresponding values are a =8.67 μm and a =3.86 μm. Both permeability formulas fit reasonably well to the simulated results, but the Happel formula, Eq. (3), leads to a more realistic hydrodynamic radius of the fibres.

PAKKA fibre-deposition model. In Fig. 3 a), we show the simulated transverse [4] and in-plane permeabilities of the PAKKA samples together with various experimental results for the transverse permeability of different materials made of artificial and natural fibres [13]. The simulated values are seen to agree very well with the experimental values in a broad range of porosity. We also see that the in-plane and transverse permeabilities of the PAKKA samples are approximately equal down to $\phi \approx 0.6$, whereas for low porosities the in-plane permeabilities are significantly smaller. This is contrary to our simulation results for the paper samples (above) and to earlier experimental results for paper [20,5]. The reason for this behavior is the rectangular cross-sectional shape and the fibre-bending mechanism used in the PAKKA model. For high values of the bending parameter (which leads to low porosity structures) the fibres become strongly bended in the z direction. As a consequence, the fibres disperse the fluid flow much more efficiently in the transverse direction making the pathlines more tortuous in the in-plane directions. This explanation is also supported by our simulations: the difference between the transverse and in-plane permeabilities was indeed found to result mostly of the assumed $k \propto 1/\tau^2$-behavior of permeability in Eq. (2); *i.e.,* substitution of the values of permeability, porosity, pore surface area and tortuosity to Eq. (2) gave relatively small variation in the Kozeny's constants c thus obtained.

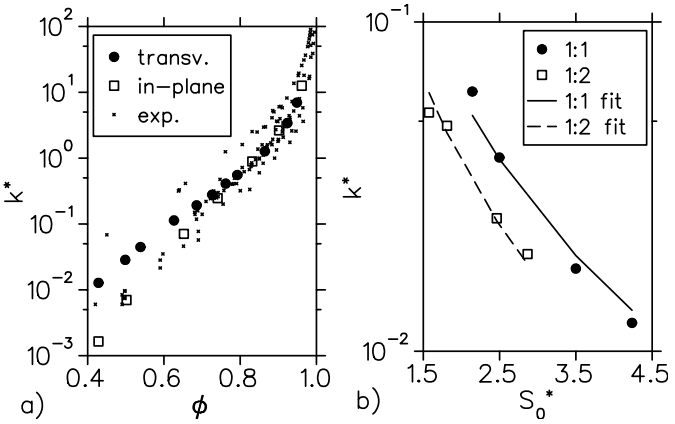

Figure 3: a) Transverse and in-plane dimensionless permeability $k^* = k/a^2$ vs. porosity ϕ for PAKKA-model samples. Here, a is the hydraulic radius of the rectangular fibres. The experimental data is for transverse permeability of various fibrous filters [13]. b) The dimensionless transverse permeability vs. dimensionless specific surface area $S_0^* = S_0 a$ at a constant porosity ϕ = 0.60 for fibres with cross-sectional height to width ratios of 1:1 and 1:2. For both shapes of fibres, the four points shown correspond to relative fines contents of 0, 10, 30 and 50 % (increasing with S_0^*). Also shown are fitted curves with $k \propto 1/S_0^2$.

In paper, fibres may be flat and contain fibrils, and the solid phase includes varying amounts of fines and fillers. In order to study the qualitative effect of these properties on transverse permeability, PAKKA samples were created with fibres of square cross section, and with fibres of flat rectangular cross section (height to width ratios of 1:1 and 1:2, respectively). Furthermore, small cubic particles with side length 1/4 of the width of the fibres were randomly deposited on pore walls.

The amount of these 'fines' particles was varied from 0 to 50 % of the total solid volume fraction which was kept at a constant value $\varphi = 0.40$. The resulting dimensionless transverse permeability, as determined by LB simulations, is shown in Fig. 3 b) [21]. The permeability is seen to decrease rapidly with increasing fines content and this behavior is very well explained by its dependence on the specific surface area, as given by the Kozeny-Carman equation, namely $k \propto 1/S_0^2$.

CONCLUSIONS

We have combined several advanced numerical and experimental techniques in analyzing flow in fibrous porous materials. The methods used include x-ray microtomography, a numerical fibre-web deposition algorithm, comprehensive 3D-image analysis, and lattice-Boltzmann flow simulations. The transverse flow permeability as determined by the lattice-Boltzmann method for fibrous mats generated by the PAKKA model, agree very well with experimental results for various fibrous materials such as filters, non-woven fabrics and stacks of cylindrical rods. The three-dimensional x-ray tomographic images of paper samples were also analyzed for the transverse and in-plane permeability, porosity, specific surface area, and tortuosity, using image-analysis methods and lattice-Boltzmann flow simulations. Although systematic comparison with experimental results has not been carried out thus far, the computed permeability of paper seems physically plausible. Furthermore, the results obtained by different methods are consistent with each other. The absolute accuracy of the computed results for paper may, however, still suffer from the limited resolution of the tomographic imaging techniques used here. For structures with larger pores and fibre dimensions, such as paper-making fabrics, tomographic imaging combined with adequate numerical simulation and analysis methods, can already lead to accurate predictions for flow permeability as well as for other transport properties.

ACKNOWLEDGEMENTS

We are grateful to Dr. Kaarlo Niskanen and Dr. Erkki Hellén (KCL) for providing us the PAKKA samples used in this work. This paper has been presented at the 2003 IPPC.

REFERENCES

1. CHOPARD, B., and DROZ, M., “Cellular automata modeling of physical systems”, Cambridge University Press, (1998).
2. ROTHMAN, D., and ZALESKI, S., “Lattice-Gas Cellular Automata: Simple Models of Complex Hydrodynamics”, Collection Al’ea. Cambridge University Press (1997).
3. FERRÉOL, B., and ROTHMAN, D. H., “Lattice-Boltzmann simulations of flow through fontainebleau sandstone” Transport in Porous Media 20 (1-2), 3 (1995).
4. KOPONEN, A., KANDHAI, D., HELLÉN, E., ALAVA, M., HOEKSTRA, A., KATAJA, M., NISKANEN, K., SLOOT, P., and TIMONEN, J., “Permeability of three-dimensional random fiber webs”, Phys. Rev. Lett. 80 (4), 716 (1998).
5. QI, D., and UESAKA, T. “Numerical Experiments On Paper-Fluid Interaction – Permeability of 3-D Anisotropic Fibre Network”, J. Materials Science 31(18), 4865 (1996).
6. NISKANEN, K. J., and ALAVA, M. J., “Planar random networks with flexible fibers”, Phys. Rev. Lett. 73, 3475 (1994).
7. ÅSTRÖM, J., MÄKINEN, J., and TIMONEN, J., “Modeling multilayer woven fabrics”, Appl. Phys. Lett. 79, 180 (2001).
8. SAMUELSEN, E. J., GREGERSEN, O. W., HOUEN, P. J., and HELLE, T., “X-ray microtomography in paper”, J. Pulp and Pap. Sci. 27 (2), 50 (2001).
9. SAMUELSEN, E. J., GREGERSEN, O. W., HOUEN, P. J., and HELLE, T.,” Three-dimensional imaging of paper by use of synchrotron X-ray microtomography”, Tappi International Paper Physics Conference, 307 (1999).
10. GUREYEV, T., EVANS, R., STEWENSON, A.W., GAO, D., and WILKINS, S. W. “X-ray phase contrast microscopy of paper”, Tappi J. 84 (2), 52 (2001).
11. GOEL, A., TZANANKAKIS, M., HUANG, S., RAMASWAMY, S., CHOI, D., and RAMARAO, B. V., “Characterization of the three-dimensional structure of paper using X-ray microtomography”, Tappi J. 84 (5), 1 (2001).
12. SCHEIDEGGER, E. A., “The Physics of Flow Through Porous Media”, Macmillan, New York (1974).
13. JACKSON, G. W., and JAMES, D. F., “The permeability of fibrous porous media”, J. Chem. Eng. 64, 364 (1986).
14. HAPPEL, J., “Viscous flow relative to arrays of cylinders”, AIChE J. 5, 174 (1959).
15. RAMASWAMY, S., HUANG S., GOEL, A., COOPER, A., CHOI, D., BANDYOBADHYAY, A., and RAMA-RAO, B. V., “The 3D structure of paper and its relationship to moisture transport in liquid and vapor forms”, In ‘The Science of Papermaking - Trans. 12th Fundamental Research Symposium’, 1289-1311, The Pulp and Paper Fundamental Research Society, Bury, Lancashire, UK (2001).
16. KOPONEN, A., KATAJA, M., and TIMONEN, J., “Tortuous flow in porous media”, Phys. Rev. E 54, 406 (1996).
17. MILLER, B., MEISER, H., “Uses of the TRI Liquid/Air Displacement Analyzer.” Tappi Nonwovens Conference, 187 (1989).
18. LINDSAY, J. D., “The Anisotropic Permeability of Paper”, Tappi J. 73 (5), 223 (1990).
19. CHOI, D., and RAMASWAMY, S., “In-plane Permeability Characteristics in Paper Board”, AIChE Symposium Series 96 (324), 80 (2000).
20. LINDSAY, J. D., and BRADY, P. H., "Studies of anisotropic permeability with applications to water removal in fibrous webs", Tappi J. 76(9), 119 (1993).
21. RASI, M., KOPONEN, A., AALTOSALMI, U., TIMONEN, J., KATAJA, M., and NISKANEN, K. J., “Permeability of paper: Experiments and numerical simulations”, Tappi International Paper Physics Conference, 297 (1999).